A systematic study of cobalt-zinc ferrite nanoparticles for self-regulated magnetic hyperthermia

P. Appa Rao [a], K. Srinivasa Rao [b, *], T.R.K. Pydi Raju [a], Govinda Kapusetti [c], Mounika Choppadandi [c], M. Chaitanya Varma [d], K.H. Rao [e]

[a] Department of Physics, DIET, Anakapalli, 531002, India
[b] Department of Physics, PBN College, Nidubrolu, 522124, India
[c] Department of Medical Devices, NIPER, Ahmadabad, 380054, India
[d] Department of Physics, GITAM (Deemed to be University), Visakhapatnam, 530045, India
[e] IIIT, RGUKT, Nuzvid, 521202, India

ARTICLE INFO

ABSTRACT

Cobalt-zinc ferrite nanoparticles having composition $Co_{1-x}Zn_xFe_2O_4$ were processed by sol-gel method with particle sizes ranging from 10.8 nm to 3.6 nm. The crystal structure, particle size, and magnetic properties were investigated by XRD, FTIR, TEM, and VSM techniques. Single domain nature was established from the coercivity versus particle size curve. The dependence of specific saturation magnetization with zinc concentration was discussed in terms of site occupancy of cations and supported by FTIR measurements. A few single domain nanoparticle compositions exhibiting low Curie temperatures and reasonably good magnetization were subjected to induction heating measurement to explore the possibility of using the materials for magnetic hyperthermia. The material, having the composition, $Co_{0.37}Zn_{0.63}Fe_2O_4$ was shown to be an excellent candidate for conducting hyperthermia study with self-regulated temperature at 46 °C.

1. Introduction

The development and characterization of magnetic nanoparticles are at their peak in recent research due to their extensive involvement in biomedical applications [1]. The magnetic nanoparticles have a greater tendency to interact with different biological entities due to their large surface area [2]. Especially, among spinel ferrite particles, low coercive single domain as well as superparamagnetic nanoparticles are promising candidates for magnetically guided drug delivery for targeting tumour, MRI signal enhancement agents, and magnetic hyperthermia mediators [3,4]. In the magnetic fluid hyperthermia treatment, nanoparticles injected into the human body interact with the cancerous cells in the affected area of the tissue and destroy the local cancerous cells without affecting the nearby normal cells through the generation of heat while the affected tissue is subjected to an external alternating magnetic field. The generation of heat associated with a nanoparticle depends on its magnetization, particle size, microstructure and loss mechanisms.

Most of the studies related to biomedical applications have focused on iron oxide nanoparticles due to their bio-compatibility [5]. Earlier reports [6] emphasized that cobalt ferrite and substituted cobalt ferrite particles having larger magnetic anisotropy are excellent candidates for biomedical applications. Ashwini B. Salunkhe et al. [7] synthesized $CoFe_2O_4$ nanoparticles with mean particle size about 10 nm through co-precipitation method for magnetic fluid hyperthermia application. AI Lehyani et al. [8] prepared nanoparticles of $CoFe_2O_4$ in the range 18—95 nm by chemical precipitation technique and observed higher heating efficiency for the particles of size 18 nm.

In performing a successful self-regulated magnetic fluid hyperthermia therapy, magnetic nanoparticles having low Curie temperatures in the temperature range 42—46° centigrade are desirable [9,10]. Despite having the privilege of heating ability, Curie temperature for most of the ferrites such as Fe_3O_4 (850 K), $MnFe_2O_4$ (580 K) and $CoFe_2O_4$ (793 K) is much higher than the required therapeutic temperature [11]. Several researchers have fabricated composite nanoparticles to obtain low Curie temperatures [12]. However, an increase in zinc concentration (x) in Me_{1-}

* Corresponding author.
E-mail address: ksr_gvsk@yahoo.co.in (K. Srinivasa Rao).

$_xZn_xFe_2O_4$ (Me = Ni, Co, Mn) nanoparticles weakens the super-exchange interaction and magneto-crystalline anisotropy in sub-lattices, and thereby producing materials of low Curie temperatures. Attaining of lower Curie temperature of a material depends on its particle size, shape, composition and the cation distribution [13,14].

Among the various ferrite compositions cited in literature, zinc substituted cobalt ferrite nanoparticles exhibiting low Curie temperature, moderate saturation magnetization; high magnetic anisotropy, low coercive single domain and superparamagnetic nature are found to be prospective candidates for hyperthermia application [1].

Efforts have been made by many researchers [15,16]in achieving least sized particles as well as improvement in the magnetic properties of the cobalt zinc nanoparticles by employing different methods of preparation. Vaidyanathan et al. [17] fabricated $Co_{1-x}Zn_xFe_2O_4$ nanoparticles through the co-precipitation technique and coated the particles with oleic acid (surfactant) for the preparation of ferro fluid. Duong et al. [18] processed superparamagnetic zinc-substituted cobalt ferrite particles of size 3 nm by forced hydrolysis method. Ibrahim Sharifi et al. [1] tried to achieve superparamagnetic behaviour in $Co_{0.3}Zn_{0.7}Fe_2O_4$ nanoparticles having Curie temperature 97 °C.

` The induction heating ability of the nanoparticles exhibits reasonable specific absorption rate along with the rise in temperature under externally applied alternating magnetic field. Nikam et al. [19] reported SAR 114.98 W/g for concentration 5 mg/mL at magnetic field (335.2 Oe) and frequency 265 kHz in nanoparticles of $Co_{0.5}Zn_{0.5}Fe_2O_4$, size about 19 nm. On the other hand, Raghavendra et al. [4] claimed higher SAR (165 W/g) for smaller superparamagnetic nanoparticles of the same composition, size around 15 nm, with lower concentrations (2 mg/mL) at magnetic field 335 Oe and frequency 267 kHz. In another report, Zhang et al. [20] synthesized $Zn_{0.54}Co_{0.46}Cr_{0.6}Fe_{1.4}O_4$nanoparticles with Curie temperature 45.7 °C and reported self-regulation of these nanoparticle suspensions to 44 °C with very low specific absorption rate 0.774 W/g. For efficient hyperthermia treatment, higher SAR values for smaller concentrations of the sample operated at low magnetic fields are desirable.

Although, there exist several reports [1,17] on the magnetic properties of cobalt-zinc ferrite nanoparticles, studies on the development of single domain cobalt-zinc nanoparticles are limited. Very few reports are available to know the role of chelating agents, particularly polyvinyl alcohol (PVA) in controlling the particle size. The induction heating experiments were conducted by earlier researchers on nanoparticles of larger size, high coercivity and high Curie temperature [20]. The said properties are undesirable for conducting magnetic hyperthermia experiments because particles of larger coercive field may cause thrombosis. Either superparamagnetic particles or low coercivity single domain magnetic nanoparticles are suggested to serve the purpose. For the first time, a systematic attempt has been made to develop single domain nanoparticles of least particle size with low Curie temperature and coercivity. The present work describes a methodical effort in exploring the effectiveness of cobalt zinc nanoparticles as potential heating agents for magnetic hyperthermia.

2. Experimental

2.1. Preparation of $Co_{1-x}Zn_xFe_2O_4$ nanoparticles

The sol-gel method was adopted in processing nanoparticles having composition $Co_{1-x}Zn_xFe_2O_4$where x varies from 0.0 to 0.8 in regular steps of 0.1. Appropriate amounts of analytical grade nitrates of ingredients were dissolved in minimum amount of de-

ionized water before making a precursor. The control of particle size has been ensured using polyvinyl alcohol as a chelating agent, keeping the ratio of weight of the composition to that of PVA at 1:3. The resulting mixture was heated at 100 °C till a gel type material was formed. The gel was dried and ground into a homogenous powder before annealing at 400 °C for an hour in air atmosphere. By adding a small amount of PVA as a binder, the ground mixture was made into toroids. Both the toroids and left-over powder of each sample were subjected to final heat treatment for another hour in the air atmosphere at 1050 °C.

2.2. Characterization

The X-ray diffraction patterns of all the samples were recorded on a powder X-ray diffractometer (BRUKER ADVANCED D8 model), employing monochromatic Cu-Kα radiation ($\lambda = 1.5406$ Å) to identify single phase spinel structures. The particle size and its distribution were determined from the transmission electron micrographs, recorded on a microscope (JOEL JEM 200CX model) operated at the electron acceleration voltage of 120 kV. In preparing a specimen for recording TEM, a drop of the ferrite powder dispersed in de-ionized water was placed on a carbon-coated copper grid and dried naturally at normal temperature. The room temperature magnetic measurements using Vibrating Sample Magnetometer (Lake Shore 7410) were carried out with a maximum applied field of 15 kOe. The Curie temperature of each sample has been estimated from the temperature dependence of magnetic permeability recorded on a toroid sample using a high frequency LCR meter (WAYNE KERR 6500 P) at 100 kHz. The induction heating ability was measured in an alternating magnetic field 20 mT at different frequencies and concentrations, using Magnetherm (make Nanotherics Limited, UK. Software - Magne Soft) by dispersing required amount of powder in 1 mL of de-ionized water.

3. Results and discussion

3.1. Identification of crystal structure

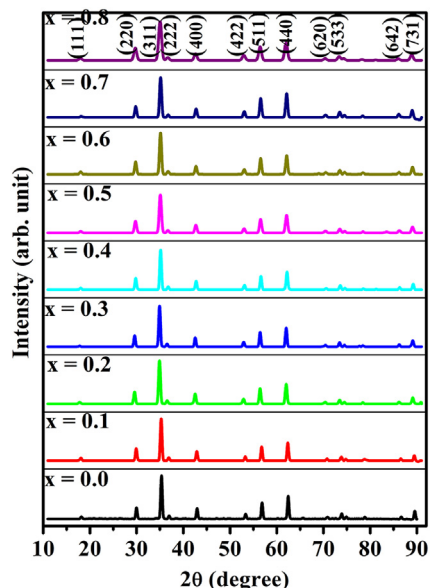The X-ray diffraction patterns of $Co_{1-x}Zn_xFe_2O_4$ nanoparticles

Fig. 1. X-ray diffraction patterns of zinc substituted cobalt ferrite.

were shown in Fig. 1. All the peaks in each pattern are in perfect agreement with those of spinel structure as substantiated with the JCPDS card (22-1086). Further, the absence of additional peaks, confirms single phase spinel structure of the final material.

3.2. Determination of particle size

Fig. 2 represents TEM images together with the particle size distribution histograms of all the zinc substituted cobalt ferrite nanoparticles. The mean particle size has been calculated using Image J software in manual mode, considering the linear size of about 120 particles taken from two image pictures of each sample by fitting the size distribution histogram with Gaussian function. A gradual decrease in estimated average particle size (from 10.8 to 3.6 nm) has been noticed with increasing zinc concentration (Table 1). Similar inferences regarding the decrease in particle size in Co-Zn nanoferrite system, prepared under different routes, were reported by several researchers [21,22].

3.3. Site occupancy of cations from VSM data

Fig. 3 shows the field dependence curves of specific saturation magnetization recorded at room temperature for cobalt-zinc nanoferrite samples heat treated at 1050 °C. Inset shows an enlarged view of the curves at origin to identify the coercive field in

Table 1
Particle size, Specific saturation magnetization, and Coercivity, for. $Co_{1-x}Zn_xFe_2O_4$ nanoparticles with zinc concentration, x.

0.0	10.8	69.7	225
0.1	8.9	72.8	318
0.2	6.9	75.7	412
0.3	6.0	79.7	275
0.4	5.0	66.1	86
0.5	4.4	62.7	79
0.6	3.6	59.6	55
0.7		Paramagnetic	
0.8		Paramagnetic	

each sample.

Table 1 gives particle size, specific saturation magnetization (σ_S), and coercivity (H_c) with zinc concentration. The specific saturation magnetization has been observed to increase with zinc concentration up to x = 0.3 followed by gradual decrease. The observed variation was in parallel to that reported by several researchers [23–25]. The measured M − H curves in case of samples having zinc concentration x = 0.7 and x = 0.8 suggest that the samples are paramagnetic. Similar measurements were reported [21,26] for higher zinc concentration in Co-Zn nanoparticles prepared by different methods.

The values of specific saturation magnetization are lower than those of the bulk counterparts [27] and the difference is attributed
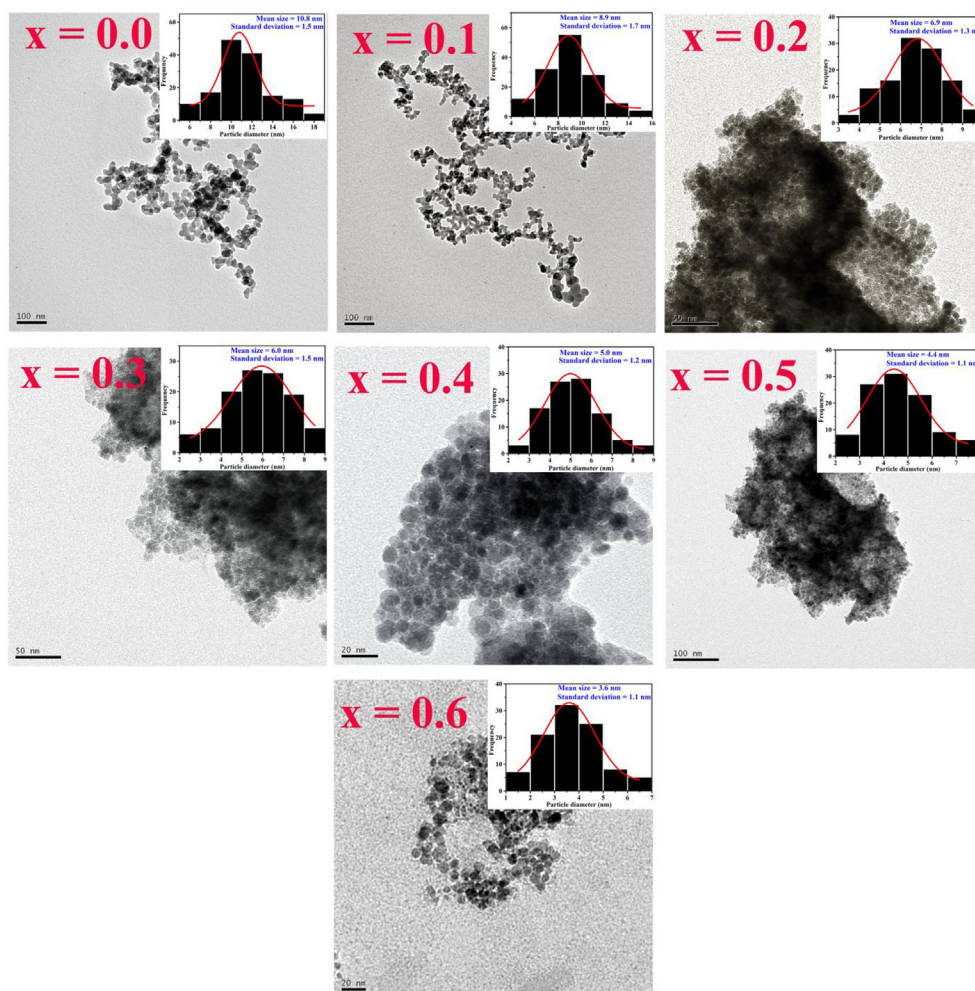

Fig. 2. TEM images and number-frequency histograms of $Co_{1-x}Zn_xFe_2O_4$ powder annealed at 1050 °C.
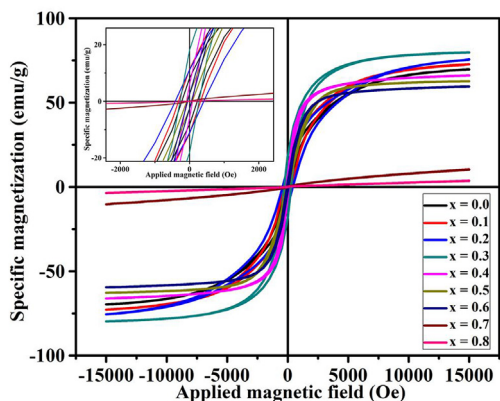
Fig. 3. Room temperature hysteresis loops of zinc substituted cobalt ferrites.

to the cation distribution and surface effects. The observed decrease in particle size with increasing zinc concentration infers that a greater number of molecules will be available on the surface of the particle which may experience different surroundings, including the existence of canted spins, the enhancement of the magnetic anisotropy, and atomic vacancies. Several experimental studies reported an increase in the effective magnetic anisotropy due to surface effects [28,29]. As the particles become smaller, the surface with the canted spins could entirely dominate the magnetic property of the nanoparticles, leading to the smaller saturation magnetization. However, the observed saturation magnetization values of the nanoferrites in the present investigation are relatively higher than those reported [30], suggesting the importance of wet chemical sol-gel process in raising the saturation magnetization.

The variation in saturation magnetization can be understood based on the exchange interactions between ions present at tetrahedral (A) and octahedral (B) sites in the spinel lattice. It is a well-known fact [31,32] that A-B exchange interaction in cobalt ferrite is predominant because nearly 20% cobalt resides on A-site. According to Néel model, A-B exchange interaction in ferrites is stronger and effective than A-A and B-B super exchange interactions and the net magnetic moment of the ferrite lattice is equal to the difference between the magnetic moments of A and B sublattices, i.e. $M = M_B - M_A$.

Because of its preference for A-sites, substitution of zinc in place of cobalt reduces the A-site magnetic moment by $2\mu_B$ until Co^{2+} ions present at A-site are depleted and this process increases the magnetic moment of B-site without affecting the A-B strong interaction. As a result, the net increase in saturation magnetization has been observed till the concentration of zinc reaches $x = 0.3$. For higher concentration beyond $x = 0.3$, zinc ions replace Fe^{3+} ions at A-sites and shift them to B-sites to replace the Co^{2+} ions at B-sites indirectly. In this process, the B-site magnetic moment increases by $3\mu_B$ and the magnetic moment of A-site decreases by $5\mu_B$. The difference in magnetic moments of A and B sites weakens A-B strong exchange interaction while promoting the intra-sublattice B-B exchange interaction, leading to a non-collinear spin arrangement of cations on B-sites. Thus, the weakening of A-B strong exchange interaction and the onset B-B interaction cause saturation magnetization to decrease with the zinc concentration. Several researchers reported the decrease in saturation magnetization with the zinc concentration for x > 0.2 considering non-collinear/canted magnetic moments [25,33]. Thus, the rise in zinc amount changes the magnetic moments of A and B sites, leading to the change from the collinear Néel's arrangement of spin moments to non-collinear Yafet-Kittel arrangement.

The dependence of specific saturation magnetization with zinc concentration can further be supported by considering the tetrahedral and octahedral band positions from FTIR measurements.

3.4. Supporting evidence from FTIR measurements

The FTIR spectra of all cobalt-zinc ferrite samples (Fig. 4) have revealed two characteristic absorption bands in the spinel structure, with the wave number range $560–594\,cm^{-1}$ and $399-420\,cm^{-1}$. The band associated with higher wave number is ascribed to the stretching vibration of $Fe^{3+} - O^{2-}$ bond at A-sites, whereas, the band with lower wavenumber, associated with the stretching vibration of $Fe^{3+} - O^{2-}$ bond at B- sites.

The respective band positions of tetrahedral and octahedral sites with zinc concentration are listed in Table 2. Insignificant variation has been observed in the wave numbers of tetrahedral and octahedral bands up to zinc concentration $x = 0.3$. Further, increase in zinc content, the tetrahedral and octahedral bands have been shifted towards the lower and higher wave numbers respectively. The gradual increase in broadening of the octahedral band beyond zinc concentration $x = 0.3$ is related to the cation redistribution in the spinel structure [23].

In general, zinc ions prefer to occupy tetrahedral, whereas, cobalt ions having a strong preference towards octahedral sites [34]. The observed change in wavenumber of the octahedral band with zinc concentration is an indication of an increase in Fe^{3+} ions in octahedral sites. In other words, the zinc ions enter A-site and push A-site iron ions into the B-site which indirectly replace the cobalt ions at B-sites. The mechanism of transferring Fe^{3+} ions (lower atomic mass) from A-site to B-site, decreases the wave number of the tetrahedral band. The mechanism involved in the displacement of Co^{2+} ion (0.745 Å) of larger ionic radius at octahedral sites with Fe^{3+} (0.645 Å) ions of smaller ionic radius and the decrease in reduced mass is responsible for the observed variation in octahedral band position. Similar result was reported in Zn substituted cobalt ferrites by Mameli et al. [35].

3.5. Single domain nature

The amount of a chelating agent and the annealing temperature play a crucial role in producing nanoparticles of smaller size. The particle size reduction is promoted in the presence of the chelating agent while crystallization and surface energy effects taking place during annealing stimulate the domain nature of the particles. Thus, the particle size decides whether it contains single domain or multi-domain natured particles. Many researchers [36,37] have studied the magnetic properties related to particle size of different nanoparticles prepared by various methods.

With increasing concentration of zinc, the probable changes in reaction kinetics prevent further growth in particle size. Several researchers have reported higher magnetization values in particles of larger size, annealed at different temperatures without altering the composition [36,38]. In our earlier publication, multi-domain ferrite nanoparticles of cobalt ferrite having size 8.1 nm with the highest specific saturation magnetization, synthesized by sol-gel method were reported [39]. However, reduction in size favours the formation of single domain particles as multi-domain formation is no longer energetically stable. Particle size reduction with the increasing zinc content was reported by several researchers in Co-Zn ferrite system [1,16,20].

The single domain nature of a given composition, in general, is established from its values of coercivity and particle size obtained at different annealing temperatures. In contrast, the single domain state, in the present investigation, was established from the values of coercivity and particle size associated with each concentration of
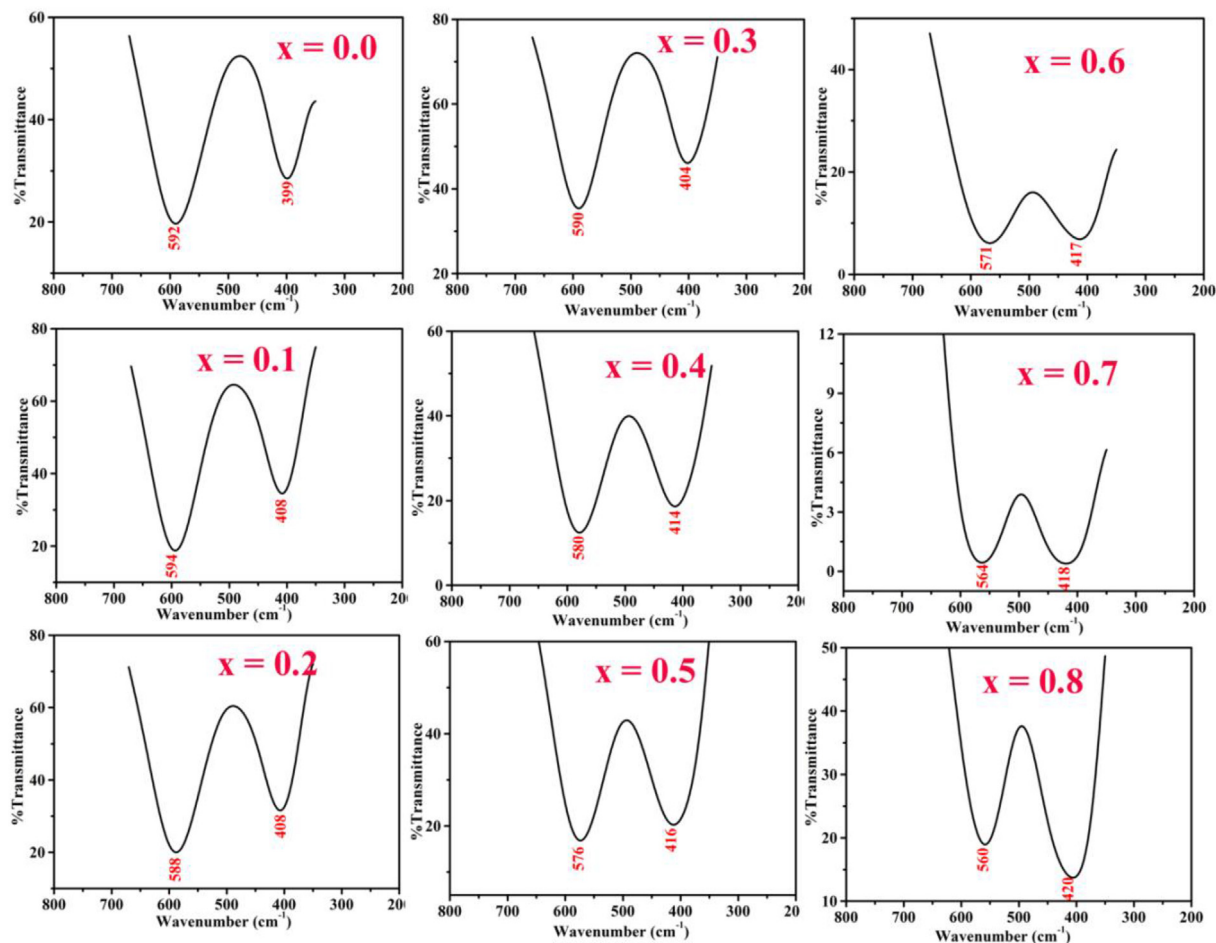
Fig. 4. Magnified pictures of absorption bands of $Co_{1-x}Zn_xFe_2O_4$.

Table 2
Band positions with zinc concentration.

Concentration x	Tetrahedral (cm^{-1})	Octahedral (cm^{-1})
0.0	592	399
0.1	594	408
0.2	588	408
0.3	590	404
0.4	580	414
0.5	576	416
0.6	571	417
0.7	564	418
0.8	560	420

zinc in $Co_{1-x}Zn_xFe_2O_4$ system, heated at 1050 °C.

Fig. 5 shows the variation of coercivity with particle size for each composition of $Co_{1-x}Zn_xFe_2O_4$. The particle size corresponds to the maximum value of coercivity is known as critical size and is around 6.9 nm. The particles below the critical size are single domain and above which are multi-domain.

The magneto-crystalline anisotropy decreases with the decrease of particle size and is comparable to thermal energy. With the application of external field, the magnetic energy aligns all the single domain particles in the direction of field. The mechanism of magnetization process is different in both single-domain and multi-domain nanoparticles. In single domain particles, the alignment is associated with the rotation of the spins while in multi-domain particles it is due to domain wall motion.
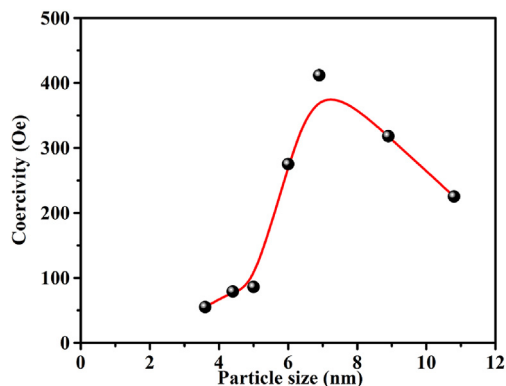

Fig. 5. Variation of coercivity with particle size.

3.6. Role of Curie temperature

The Curie temperature of each sample has been estimated from the plots of temperature dependence of initial permeability (Fig. 6), recorded on a toroid sample using a high frequency LCR meter at 100 kHz. The temperature at which a sudden fall of initial permeability takes place is known as Curie temperature.

Fig. 7 shows the variation of the Curie temperature with zinc concentration. In explaining the observed variation in Curie temperature with zinc concentration, exchange interaction between
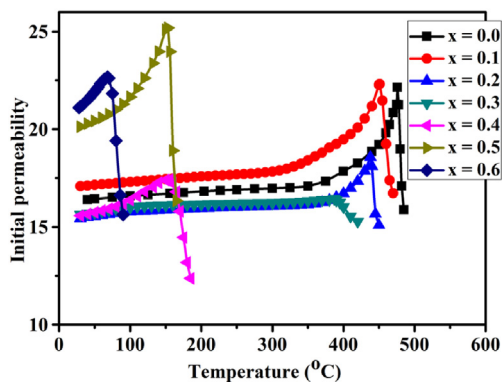
Fig. 6. Variation of initial permeability with temperature in $Co_{1-x}Zn_xFe_2O_4$.
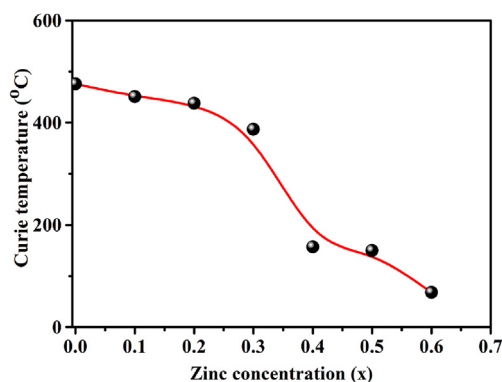

Fig. 7. Variation of Curie temperature with zinc concentration (x).

magnetic ions and their site occupancy was considered. As zinc ions prefer to occupy tetrahedral sites, Co^{2+} ions existing at A-site in cobalt ferrite are replaced by zinc up to its concentration x = 0.2 without much affecting strong A-B exchange interaction. During this process, a gradual decrease in Curie temperature with zinc concentration is expected due to the decrease in the overall magnetic moment of the unit cell. Beyond the zinc concentration x = 0.2, zinc ions continue to occupy A-site and replace cobalt ions at B-sites indirectly by shifting A site ferric ions to B site. The process dilutes the magnetic moment of the A-sub lattice, increases the magnetic moment of the B-site and apparently weakens the A-B exchange interaction. The sudden decrease in Curie point with the increase in zinc content is a clear evidence of the onset of the B-B interaction which has been a well-known phenomenon [40].

Interestingly, the observed decrease in Curie temperature and coercivity with increasing zinc concentration guided the authors to process a few compositions in between x = 0.6 and 0.7 to check their suitability for studying magnetic hyperthermia. Three samples having zinc concentration x = 0.61, 0.62 and 0.63 were carefully prepared to record the induction heating measurements. The values of specific saturation magnetization, coercivity and Curie temperature are shown in Table 3.

Table 3
Specific saturation magnetization (σ_S), Curie temperature, Coercivity (H_c) of $Co_{1-x}Zn_xFe_2O_4$ with zinc concentration, x.

x	σ_S (emu/g)	H_c (Oe)	Curie temperature (°C)
0.61	50.5	29	65
0.62	43.1	16	55
0.63	38.7	10	46

4. Magnetic hyperthermia experiment

Because of its single domain nature, reasonably high specific saturation magnetization, and low Curie temperature, the composition $Co_{0.4}Zn_{0.6}Fe_2O_4$ has been subjected to induction heating to analyse the concept in the first instance. Self-heating characteristics of the sample dispersed in de-ionized water medium has been recorded under the application of alternating magnetic field of 20 mT at different frequencies keeping the sample concentration 10 mg/mL. The temperatures versus time curves are given in Fig. 8.

A sharp initial raise followed by a gradual increase in temperature with time has been observed until the temperature reaches the Curie temperature of the sample and remains constant. This kind of observation is very much evident in case the sample is run at high frequency because the rapid increase in temperature is observed to be dependent on the frequency selected. The higher the frequency, greater the temperature rise.

In the process of induction heating, the temperature rise with time is attributed to magnetic losses in the material. Eddy current losses are ignored primarily due to high resistivity of the particles. In general, single domain nanoparticles below the critical particle size produce heating mechanism due to Brownian loss, whereas multi-domain particles are associated with both Néel and Brownian losses in generating heat. Néel loss is due to domain wall displacement and the impediment of particles due to liquid viscous force causes Brownian loss [41]. As the sample, $Co_{0.4}Zn_{0.6}Fe_2O_4$ exhibits coercivity 55 Oe, the heat generated has been presumed to include a partial contribution from hysteresis loss besides the Brownian and/or Néel mechanisms.

Kim et al. [42] studied the heating ability of various ferrite nanoparticles in distilled water under alternating magnetic field of frequency about 7 MHz with field amplitude 110 A/m. Veverka et al. [43] performed magnetic heating experiments on the cobalt ferrite nanoparticles, suspended in agarose solid gel in the range of alternating field from 35 mT to 80 mT at frequency 108 kHz. Dong-Hyun Kim et al. [44] carried out the heat generation in cobalt ferrite nanoparticles dispersed in water by applying various magnetic fields from 127 Oe to 634 Oe at frequencies of 231 and 266 kHz. Zhang et al. [20] conducted magnetic heating experiment in Co-Zn-Cr ferrite nanoparticles of coercivity 174 Oe using high concentration, 112 mg/mL of the sample. Although the temperature was regulated at 44 °C, the particles are neither single domain nor superparamagnetic.

As the Curie temperature of $Co_{0.4}Zn_{0.6}Fe_2O_4$ is above the therapeutic range 68 °C, the induction heating experiment has been extended to three more compositions, $Co_{0.39}Zn_{0.61}Fe_2O_4$, $Co_{0.38}Zn_{0.62}Fe_2O_4$ and $Co_{0.37}Zn_{0.63}Fe_2O_4$ which have low Curie
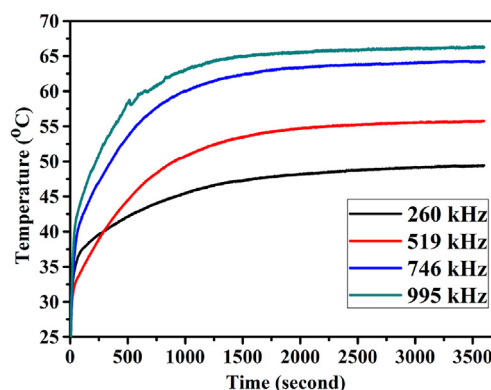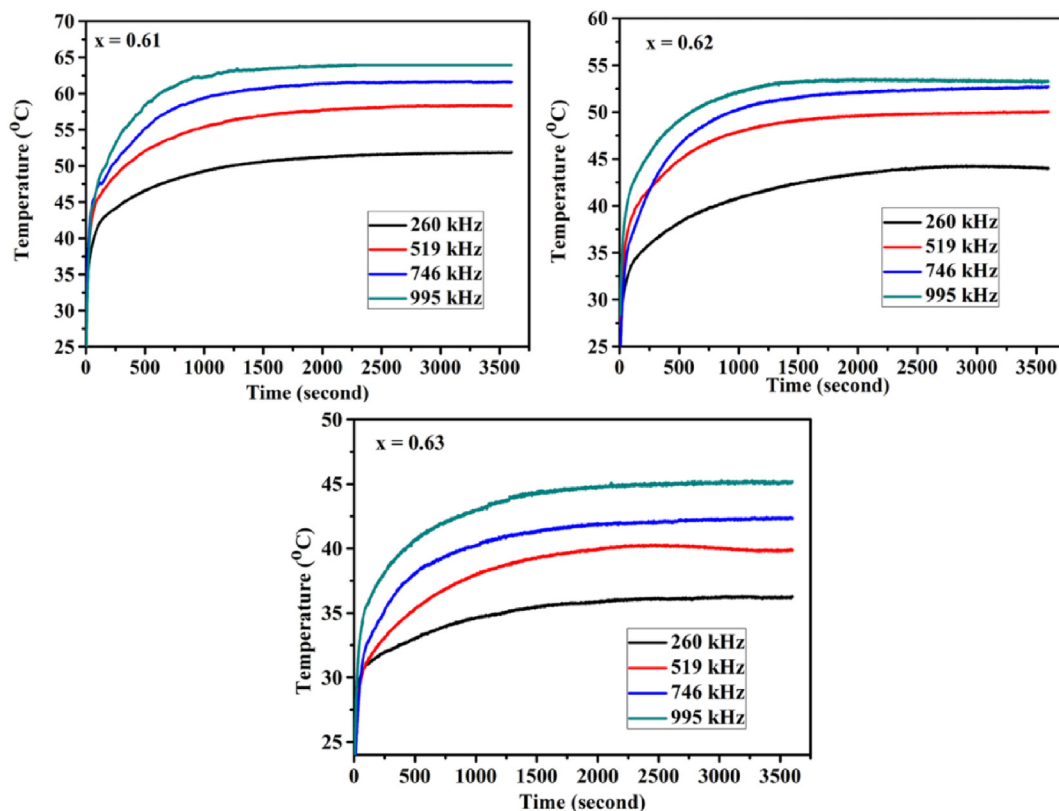

Fig. 8. Temperature variation with time of $Co_{0.4}Zn_{0.6}Fe_2O_4$.

Fig. 9. Heating abilities of $Co_{1-x}Zn_xFe_2O_4$ nanoparticles at various frequencies.

temperatures (Table 3). The temperature versus time curves for the three samples are given in Fig. 9.

In the present study, the applied field 20 mT which is lower than that reported by other researchers. From the above experimental data, it is clearly seen that the composition $Co_{0.37}Zn_{0.63}Fe_2O_4$ having the least coercivity (10 Oe) and low Curie temperature (46 °C) provides the required therapeutic temperature range 42—46 °C for more than 30 min at higher frequency 995 KHz. More amount of the sample dispersed in water may yield the required temperature range even at lower frequency (Fig. 10).

The experiments conducted at different frequencies with the varied amounts of the sample dispersed in water medium have concluded that the heating ability would be intensified with higher amount dispersed, and higher frequency of operation. In hyperthermia experiments, in general, the conditions needed to obtain the required therapeutic temperature range are the application of minimum applied alternating magnetic field, medium frequency and smaller amount of the material dispersed in water medium. In general, the therapeutic range 41—46 °C is expected for at least 30 min above the frequency 500 KHz.

Depending upon the situation of the tissue under study, one must select the proper values of applied alternating field; frequency of operation and the amount of the sample to be administered to obtain the required therapeutic temperature range at the site of the tissue.
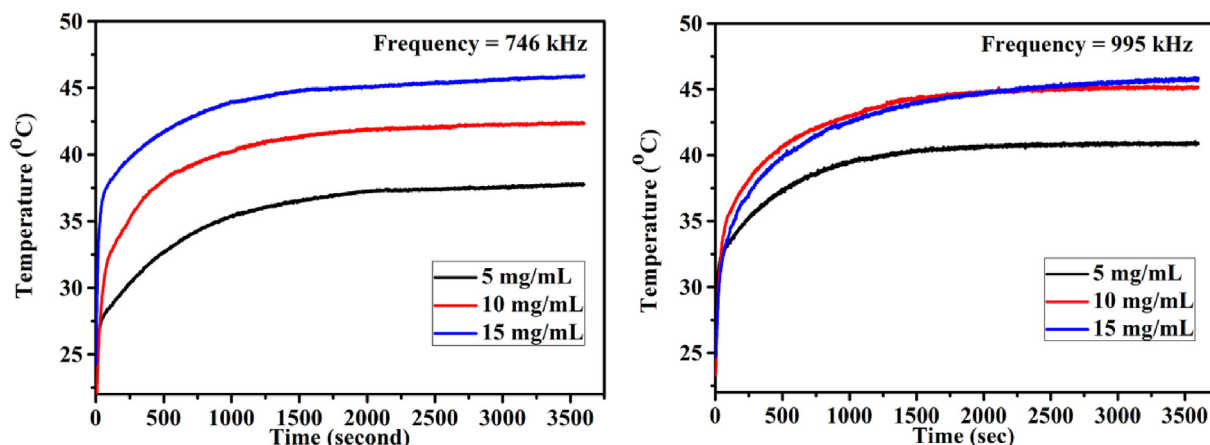

Fig. 10. Heating abilities of $Co_{1-x}Zn_xFe_2O_4$ nanoparticles for various concentrations at two frequencies.

5. Conclusion

In cobalt-zinc nanoferrite system, the importance of the zinc concentration in producing the particles of least size with fascinating properties, suitable for magnetic hyperthermia has been discussed in detail. The study has revealed that least sized nanoparticles with reasonably high specific saturation magnetization, low coercivity and low Curie temperatures can be made available by the sol-gel method. Induction heating study of such particles confirms their suitability for magnetic hyperthermia treatment. The material having the composition $Co_{0.37}Zn_{0.63}Fe_2O_4$ has been proved to be a promising candidate for conducting hyperthermia experiments with the attainment of self-regulation at $46\,°C$ due to its low Curie temperature ($46\,°C$).

Acknowledgements

References

[1] Ibrahim Sharifi, H. Shokrollahi, J. Magn. Magn. Mater. 324 (2012) 2397—2403.
[2] Chaitali Deya, Kaushik Baishya, Arup Ghosh, Madhuri Mandal Goswami, Ajay Ghosh, Kalyan Mandal, J. Magn. Magn. Mater. 427 (2017) 168—174.
[3] Katerina Hola, Zdenka Markova, Giorgio Zoppellaro, Jiri Tucek, Radek Zboril, Biotechnol. Adv. 33 (2015) 1162—1176.
[4] A. Bohara Raghvendra, Nanasaheb D. Thorat, Akhilesh K. Chaurasia, Shivaji H. Pawar, RSC Adv. 5 (2015) 47225—47234.
[5] Ajay Kumar Gupta, Mona Gupta, Biomaterials 26 (2005) 3995—4021.
[6] Ibrahim Sharifi, H. Shokrollahi, S. Amiri, J. Magn. Magn. Mater. 324 (2012) 903—915.
[7] Ashwini B. Salunkhe, Vishwajeet M. Khot, Juan M. Ruso, S.I. Patil, J. Magn. Magn. Mater. 419 (2016) 533—542.
[8] S.H.A. Al Lehyani, R.A. Hassan, A.A. Alharbi, T. Alomayri, H. Alamri, Int. J. Adv. Technol. 8 (2017) 6, https://doi.org/10.4172/0976-4860.1000196.
[9] Wei Zhang, Chengwei Wu, S. Ravi, P. Silva, Expert Rev. Anticancer Ther. 18 (8) (2018) 723—725.
[10] R. Arulmurugan, B. Jeyadevan, G. Vaidyanathan, S. Sendhilnathan, J. Magn. Magn. Mater. 288 (2005) 470—477.
[11] Zhila Shaterabadi, Gholamreza Nabiyouni, Meysam Soleymani, Prog. Biophys. Mol. Biol. 133 (2018) 9—19.
[12] I. Apostolova, J.M. Wesselinowa, Solid State Commun. 149 (2009) 986—990.
[13] Y. Haik, V. Mohite, C.J. Chen, Nanotechnology 1 (2005) 300—303.
[14] T.N. Brusentsova, N.A. Brusentsov, V.D. Kuznesov, V.N. Nikiforov, J. Magn. Magn. Mater. 293 (2005) 298—302.
[15] M. BenAli, K. El Maalam, H. El Moussaoui, O. Mounkachi, M. Hamedoun, R. Masrour, E.K. Hlil, A. Benyoussef, J. Magn. Magn. Mater. 398 (2016) 20—25.
[16] J. López, L.F. González-Bahamón, J. Prado, J.C. Caicedo, G. Zambrano, M.E. Gómez, J. Esteve, P. Prieto, J. Magn. Magn. Mater. 324 (2012) 394—402.
[17] G. Vaidyanathan, S. Sendhilnathan, Physica B 403 (2008) 2157—2167.
[18] G.V. Duong, N. Hanh, D.V. Linh, R. Groessinger, P. Weinberger, E. Schafler, M. Zehetbauer, J. Magn. Magn. Mater. 311 (2007) 46—50.
[19] D.S. Nikam, S.V. Jadhav, V.M. Khot, M.R. Phadatare, S.H. Pawar, J. Magn. Magn. Mater. 349 (2014) 208—213.
[20] Wei Zhang, Xudong Zuo, Ying Niu, Chengwei Wu, Shuping Wang, Shui Guan, S. Ravi, P. Silva, Nanoscale 9 (2017) 13929—13937.
[21] M.A. Gabal, A.A. Al-Juaid, S.M. Al-Rashed, M.A. Hussein, F. Al-Marzouki, J. Magn. Magn. Mater. 426 (2017) 670—679.
[22] N.M. Deraz, A. Alarifi, J. Anal. Appl. Pyrolysis 94 (2012) 41—47.
[23] M. Chithra, C.N. Anumol, Baidyanath Sahu, Subasa C. Sahoo, J. Magn. Magn. Mater. 424 (2017) 174—184.
[24] Mircea Stefanescu, Marius Bozdog, Cornelia Muntean, Oana Stefanescu, Titus Vlase, J. Magn. Magn. Mater. 393 (2015) 92—98.
[25] R. Topkaya, A. Baykal, A. Demir, J. Nanoparticle Res. 15 (2013) 1359. https://doi.org/10.1007/s11051-012-1359-6.
[26] Charanjit Singh, Sheenu Jauhar, Vinod Kumar, Jagdish Singh, Sonal Singhal, Mater. Chem. Phys. 156 (2015) 188—197.
[27] A. Hassadee, T. Jutarosaga, W. Onreabroya, Proc. Eng. 32 (2012) 597—602.
[28] M. Jamet, W. Wernsdorfer, C. Thirion, D. Mailly, V. Dupuis, P. Mélinon, A. Pérez, Phys. Rev. Lett. 86 (2001) 4676—4679.
[29] Matthieu Jamet, Wolfgang Wernsdorfer, Christophe Thirion, Véronique Dupuis, Patrice Mélinon, Alain Pérez, Dominique Mailly, Phys. Rev. B 69 (2004), 024401.
[30] E. Hema, A. Manikandan, P. Karthika, S. Arul Antony, B.R. Venkatraman, J. Supercond. Nov. Magnetism 28 (2015) 2539—2552.
[31] K. Srinivasa Rao, P. Appa Rao, M. Chaitanya Varma, K.H. Rao, J. Alloys Compd. 750 (2018) 838—847.
[32] K. Srinivasa Rao, A. Mahesh Kumar, M. ChaitanyaVarma, G.S.V.R.K. Choudary, K.H. Rao, J. Alloys Compd. 488 (2009) L6—L9.
[33] Dipali S. Nikam, Swati V. Jadhav, Vishwajeet M. Khot, R.A. Bohara, Chang K. Hong, Sawanta S. Mali, S.H. Pawar, RSC Adv. 5 (2015) 2338—2345.
[34] A.V. Raut, R.S. Barkule, D.R. Shengule, K.M. Jadhav, J. Magn. Magn. Mater. 358—359 (2014) 87—92.
[35] V. Mameli, A. Musina, A. Ardu, G. Ennas, D. Peddis, D. Niznansky, C. Sangregorio, C. Innocenti, Nguyen T.K. Thanh, C. Cannas, Nanoscale 8 (2016) 10124—10137.
[36] Mehrnaz Gharagozlou, J. Alloys Compd. 486 (2009) 660—665.
[37] B.G. Toksha, Sagar E. Shirsath, S.M. Patange, K.M. Jadhav, Solid State Commun. 147 (2008) 479—483.
[38] Lunhong Ai, Jing Jiang, Curr. Appl. Phys. 10 (2010) 284—288.
[39] K. Srinivasa Rao, S.V. RangaNayakulu, M. Chaitanya Varma, G.S.V.R.K. Choudary, K.H. Rao, J. Magn. Magn. Mater. 451 (2018) 602—608.
[40] H.H. Joshi, P.B. Pandya, K.B. Modi, N.N. Jani, G.J. Baldha, R.G. Kulkarni, Bull. Mater. Sci. 20 (1997) 93—101.
[41] D. Ortega, Q.A. Pankhurst, Nanoscience, vol. 1, Nanostructures through Chemistry, 2013, pp. 60—88.
[42] Dong-Hyun Kim, Se-Ho Lee, Kyoung-Nam Kim, Kwang-Mahn Kim, In-bo Shim, Yong-Keun Lee, J. Magn. Magn. Mater. 293 (2005) 320—327.
[43] M. Veverka, P. Veverka, O. Kaman, A. Lančok, K. Závěta, E. Pollert, K. Knížek, J. Boháček, M. Beneš, P. Kašpar, E. Duguetand, S. Vasseur, Nanotechnology 18 (2007) 345704, 7pp.
[44] Dong-Hyun Kim, David E. Nikles, Duane T. Johnson, Christopher S. Brazel, J. Magn. Magn. Mater. 320 (2008) 2390—2396.